Chinese Journal of
POLYMER SCIENCE

RESEARCH ARTICLE

https://doi.org/10.1007/s10118-026-3762-y
Chinese J. Polym. Sci.

Effect of Graphene/Nickel-iron Layered Double Hydroxide Hybrids on the Thermal Decomposition and Flame Retardancy of Acrylonitrile-butadiene-styrene Copolymer Composites

Ning-Ning Hong[a], Jing-Ping Liu[a], and Xin Wang[b*]

[a] *State Key Laboratory of High-Efficiency Special Cable Technology, Shanghai Electric Cable Research Institute Co., Ltd., Shanghai 200093, China*
[b] *State Key Laboratory of Fire Science, University of Science and Technology of China, Hefei 230026, China*

Electronic Supplementary Information

Abstract A novel synergistic structure (GNS-LDH) was synthesized by modifying graphene with Ni/Fe layered double hydroxide hybrids *via* hydrothermal method, which have successfully constructed high-performance acrylonitrile butadiene styrene (ABS) nanocomposites in terms of strength, toughness, and smoke toxicity safety through solution blending technology. The composites exhibited excellent mechanical properties, with a tensile strength of 46.23 MPa, elongation at break of 5.78%, and flexural strength of 53.16 MPa. In terms of flame retardancy, the heat release rate of the composites was reduced by 33.2% and the total heat release was reduced by 12.3% with the addition of 2.0 wt% GNS-LDH. Moreover, the generation of toxic gases, such as CO, CO_2 and HCN, during the combustion process was effectively suppressed, and the smoke generation rate was significantly reduced. The comprehensive performance of this ABS nanocomposite based on GNS-LDH in terms of enhancement and toughening, flame retardancy, smoke suppression, and reduction in toxicity has surpassed that of many similar materials reported in the current literature, which provides a new way of thinking for the design and development of high-performance protective materials.

Keywords Novel synergistic structure; Mechanical enhancement; Flame retardant; Thermal stability

Citation: Hong, N. N.; Liu, J. P.; Wang, X. Effect of graphene/nickel-iron layered double hydroxide hybrids on the thermal decomposition and flame retardancy of acrylonitrile-butadiene-styrene copolymer composites. *Chinese J. Polym. Sci.* https://doi.org/10.1007/s10118-026-3762-y

INTRODUCTION

Acrylonitrile-butadiene-styrene (ABS) copolymers are excellent thermoplastic polymers for a wide range of automotive, electronic, and construction applications. It has good mechanical properties, easy processing and excellent chemical resistance, but ABS is flammable and releases large amounts of toxic gases, such as CO and HCN, during combustion, which is a serious safety hazard.[1] The traditional flame-retardant method involves the addition of halogenated flame retardants, which can improve the flame retardant properties. Combustion results in the production of large amounts of smoke and toxic gases, and halogenated compounds may harm the environment and human health.[2] Inorganic layered materials have shown significant advantages over flame-retardant polymers.[3] However, it is difficult to meet the demand for high-performance flame-retardant materials for ABS because of the limited dispersion of inorganic fillers in the matrix and the inherent limitations of their flame-retardant efficiency, large number of additives, and significant impact on the mechanical properties of the materials.

Layered double hydroxide (LDH) have attracted much attention recently because of their hydrotalcite-like structure and unique properties. It is formed by replacing some divalent cations with trivalent cations *via* intercalation, thus providing compositional tunability and flexible ion-exchange capabilities.[4,5] In the field of flame retardancy, LDH, particularly those containing transition metal elements such as iron and nickel, have shown high efficiency in reducing polymer fire hazards by facilitating char formation during polymer degradation.[6–8] An *et al.* synthesized caprolactam-modified three-dimensional floral templated layered double hydroxides (LDHs) and reduced graphite oxide (rGO) and applied them to composite emulsions, which reduced the leather emulsion heat release rate and smoke generation rate of leather latex and significantly improved the flame retardant and smoke inhibition properties.[9] Song *et al.* constructed defective Co-LDH@ZIF-67 (d-LDH@ZIF) heterostructures *in situ* using Co-LDH as the sacrificial template and carrier.[10] The presence of many cobalt/oxygen vacancies and lattice defects in the heterostructure endows it with better catalytic performance. When applied to polyurea composites, they have obvious advantages in terms of flame retardancy and mechanical properties. However, similar to graphene, high-charge-density LDHs suffer from aggregation problems and

* Corresponding author, E-mail: wxcmx@ustc.edu.cn
Received March 2, 2026; Accepted May 29, 2026; Published online July 24, 2026

their dispersion in a polymer matrix remains a challenge.

Graphene oxide (GO), with its large specific surface area and multiple functionalized substrates, is an ideal carrier for building nanomaterials.[11] Combining LDH with GO can endow graphene with a larger specific surface area and desirable electrical conductivity and capacitance, allowing it to be widely used as an electrode material for lithium batteries or supercapacitors.[12,13] In addition, the combination of graphene with LDH is expected to play an important role in enhancing flame-retardant polymers. On the one hand, the introduction of LDH on the graphene surface can inhibit the aggregation of graphene, which improves the dispersion of the blends in the matrix and enhances the mechanical properties of the composites. On the other hand, hybrid materials can synergize the physical barrier effect of graphene with the thermal desorption heat and catalytic effect of LDH, thus exploiting the advantages of both materials in the flame-retardant field. For example, 8-hydroxyquinoline (8-HQ)-intercalated CaAl-based bilayer hydroxide (CaAl-8HQ-LDH) was loaded onto reduced GO (rGO) and used as a nanofiller, which imparts excellent flame retardancy to epoxy resin (EP/CaAl-8HQ LDH@rGO) and ensures the effective protection of mild steel.[14] The multifunctional additive piperazine pyrophosphate@layered double hydroxide@reduced graphene oxide (PPAP@LDH@rGO), which has a layered core-shell structure, was constructed *via* solvothermal and electrostatic self-assembly methods.[15] Owing to the synergistic effect of PPAP, LDH and rGO, the EP thermoset material achieved a UL-94 V-0 rating with an ultimate oxygen index of 29.8% in the vertical combustion test. During the combustion process, EP/PPAP@LDH@rGO significantly reduced the release of smoke and harmful products such as carbon monoxide. In addition, the EP thermosets maintained good electrical insulation and mechanical properties.

Based on the synergistic effect of graphene and nickel-iron layered double hydroxide (LDH), we prepared a high-performance ABS nanocomposite *via* an *in situ* hydrothermal method and a solution blending strategy. This nanocomposite combines the advantages of NiFe-LDH and reduced graphene oxide (GNS), and its structure is designed such that the NiFe-LDH nanosheets are tightly anchored on the surface of the GNS to form a unique two-dimensional hybrid architecture, which effectively inhibits the agglomeration phenomenon of the graphene flakes and greatly expands their dispersion in the polymer matrix. Moreover, the introduction of GNS-LDH hybrids into the ABS matrix not only significantly enhanced the mechanical properties, with a tensile strength as high as 46.23 MPa and elongation at break as high as 5.78%, but also led to an overall improvement in the thermal stability and flame retardancy of the material. Thermogravimetric analysis revealed that the thermal decomposition temperature of the ABS/GNS-LDH composite was moderately reduced, but the final residual char amount was significantly increased, indicating that it could form an effective protective char layer at high temperatures. More importantly, the release of toxic gases from the composite during combustion was significantly reduced, with a 33.2% reduction in the heat release rate (PHRR) and a 12.3% reduction in the total heat release (THR). This is strong evidence of the excellent efficacy of GNS-LDH hybrids in enhancing the fire safety of ABS materials.

EXPERIMENTAL

Materials

The materials used in this study are listed in the electronic supplementary information (ESI).

Synthesis of GNS-LDH

Graphite oxide (GO) was obtained by oxidizing expandable graphite *via* the Hummers method. GNS-LDH hybrids (Ni/Fe molar ratio of 4) were prepared in one step *via* an in situ hydrothermal method as follows: GO was dissolved in 80 mL of deionized water and ultrasonicated for 30 min. Then, $Ni(NO_3)_2{\cdot}6H_2O$, Fe, $Ni(NO_3)_2{\cdot}6H_2O$, $Fe(NO_3)_3{\cdot}9H_2O$ and urea were added after 30 min of ultrasonication, and the concentrations of the three were controlled to be 16, 4 and 35 mmol/L, respectively. Sodium citrate was subsequently added to the above mixture and magnetically stirred for 2 h at room temperature, after which the mixture was transferred to a polytetrafluoroethylene-lined high-pressure reactor and allowed to react at 160 °C for 48 h. The hydrothermal reaction was carried out for 48 h. The reaction was carried out in the same way as the hydrothermal reaction. At the end of the hydrothermal reaction, the slurry was centrifuged, washed with a large amount of deionized water and ethanol and collected. For comparison, GNS were obtained by hydrothermal treatment of GO under the same conditions.

Preparation of ABS/GNS-LDH Nanocomposites

Owing to the high interlayer force and easy agglomeration of the graphene sheets, the ABS/GNS-LDH composites were prepared *via* a solution blending method. The GNS-LDH slurry was added to 200 mL of acetone and sonicated for 30 min to form a suspension. ABS particles were then added to the solution and mechanically stirred. The mixture was heated to 70 °C and refluxed for 4 h. The mixture was then poured into an open petri dish and dried in a vacuum oven for 12 h. Finally, the resulting ABS composites were placed at 205 °C and 10 MPa for 15 min to obtain flakes of suitable thickness. For comparison, the ABS/GNS composites were prepared using the same procedure. All composite formulations are listed in Table 1.

Characterization

The instruments and related characterization methods used in this study are listed in ESI.

RESULTS AND DISCUSSION

Morphological and Structural Characterization of GNS-LDH

Fig. 1 shows a schematic of the process of synthesizing GNS-LDH hybrids *via* an *in situ* hydrothermal method and preparing ABS/GNS-LDH composites *via* the solution blending method.[16] First, Ni^{2+}, Fe^{3+} and GO formed a homogeneous aqueous solution, and Ni^{2+} and Fe^{3+} were adsorbed on the GO surface due to the electrostatic force of attraction between the metal cations and the hydroxyl and carboxyl groups on the GO surface. When the system reacts for a long time at 160 °C, urea is hydrolyzed by heat, and the generated alkali reacts with Ni^{2+} and Fe^{3+} to form

Table 1 Compositions of ABS nanocomposites with GNS and GNS-LDH and their tensile and bending properties.

Sample	ABS (wt%)	GNS (wt%)	GNS-LDH (wt%)	Tensile strength (MPa)	Elongation at break (%)	Bending strength (MPa)
ABS	100			28.84	27.96	39.00
ABS/GNS0.5	99.5	0.5		36.05	6.54	43.57
ABS/GNS1	99	1		37.38	1.68	51.71
ABS/GNS2	98	2		37.53	2.76	53.71
ABS/GNS-LDH0.5	99.5		0.5	41.16	6.43	48.44
ABS/GNS-LDH1	99		1	46.23	5.78	53.16
ABS/GNS-LDH2	98		2	45.23	2.16	56.79

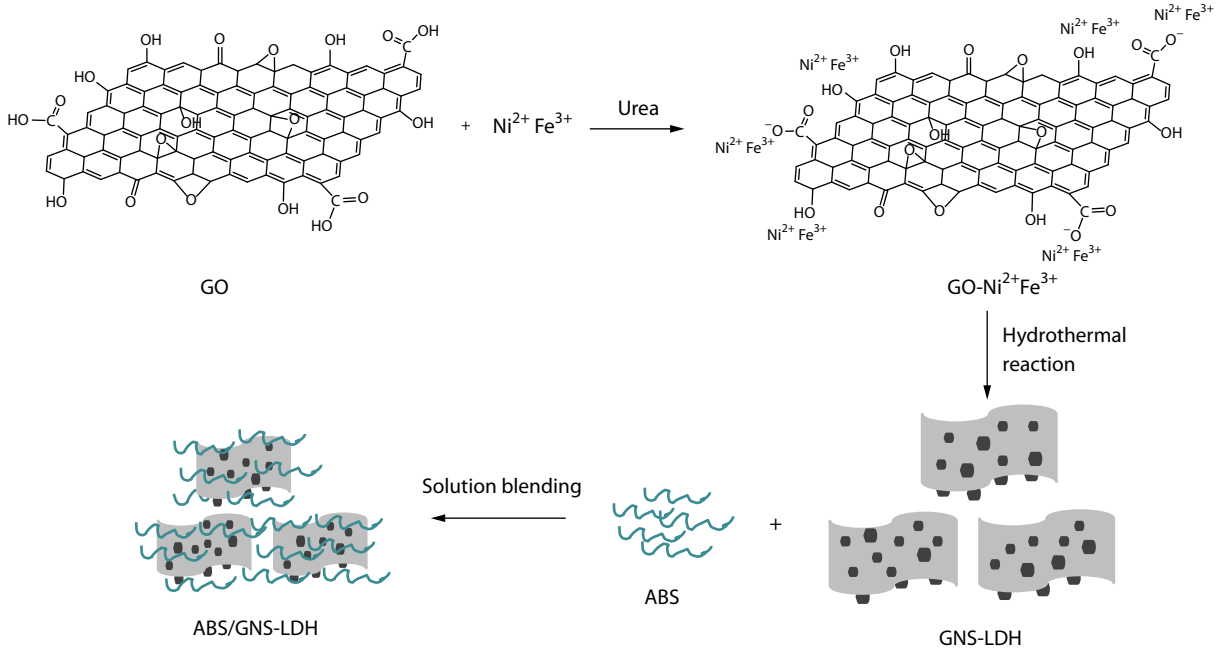

Fig. 1 Schematic outline of the preparation of the GNS-LDH hybrid and its ABS composite.

NiFe-LDH nuclei. Moreover, under high-temperature hydrothermal conditions, GO was reduced to GNS using urea, and the agglomeration of GNS was suppressed to a certain extent because of the uniform distribution of NiFe-LDH on the surface of the GNS. The heterocompounds were dispersed *via* ultrasonication to form a suspension in the solution, and then the ABS polymer was added. Under constant stirring and heating, the ABS polymer chains were adsorbed and inserted into the graphene flakes, and the polymer was sandwiched between the GNS-LDH layers to form an ABS/GNS-LDH composite material after the solvent was removed.

Fig. 2(a) shows the Raman spectra of GO, GNS, and GNS-LDHs. The increase in the I_D/I_G ratio for GNS compared with that for GO may be due to the smaller size of graphene and the defects introduced into the structure by hydrothermal reduction.[17] GNS-LDH has weak D- and G-band peaks, which may be due to the attachment of NiFe-LDH, resulting in disorganization of the conjugated structure of graphene. Raman peaks located at 198, 297, 465, 538, and 671 cm^{-1}, corresponding to the vibrations of Ni—O and Fe—O in NiFe-LDH, were also observed.[18] The morphological features of GNS and GNS-LDHs were observed by TEM. As shown in Fig. 2(b), the GNS had a lamellar structure with a size of more than a few micrometers, and there was also a stacking phenomenon in the local area. As shown in Fig. 2(c), many NiFe-LDH nanosheets are uniformly distributed on the GNS surface. Owing to the domain-limiting effect of GNSs, the size of NiFe-LDH was small and the particle size distribution was narrow (6–14 nm). The stacking of GNSs was effectively avoided because of the surface loading of the NiFe-LDH nanosheets. HRTEM characterization of GNS-LDH revealed that the lattice stripes of the loaded nanoparticles had a spacing of 0.23 nm, which corresponds to the (015) plane of LDH (Fig. 2d).[19]

Fig. 3 shows AFM images and profile height maps of GO, GNS, and GNS-LDH (c). Fig. 3(a) shows that GO is a large and thin sheet material with a size of a few micrometers or more and thickness of approximately 1.1 nm. The GNS, on the other hand, has a curled and twisted morphology with a thickness of several tens of nanometers, indicating severe agglomeration (Fig. 3b). For GNS-LDH, the surface appeared rough owing to the attachment of NiFe-LDH nanosheets. The profile height map indicated that the nanoparticle size was approximately 8.2 nm and that there was no obvious agglomeration owing to the presence of GNSs, although the NiFe-LDH stacking density was high (Fig. 3c).

Dispersion of GNS-LDH in ABS

Graphene is well dispersed in the matrix and strongly interacts with the matrix to significantly improve the properties of composites.[20] Fig. 4 shows the ABS composite films obtained *via* the solution blending method. The pure ABS film is light yellow

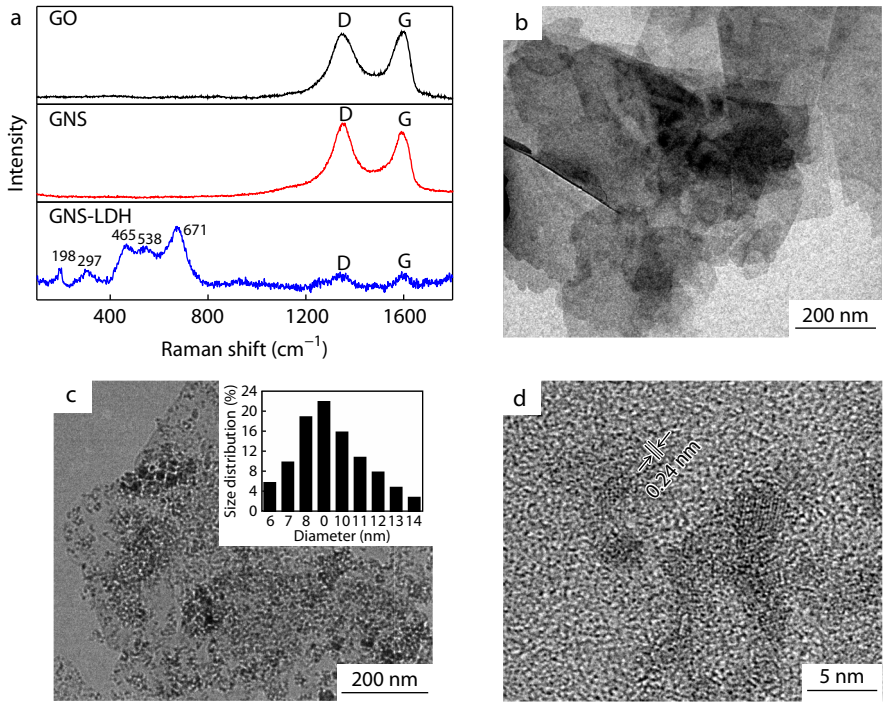

Fig. 2 (a) Raman spectra of GO, GNS and GNS-LDH; TEM images of (b) GNS and (c) GNS-LDH, and (d) HRTEM image of GNS-LDH. The inset in (c) shows the size distribution of NiFe-LDH nanoparticles on the GNS sheets.

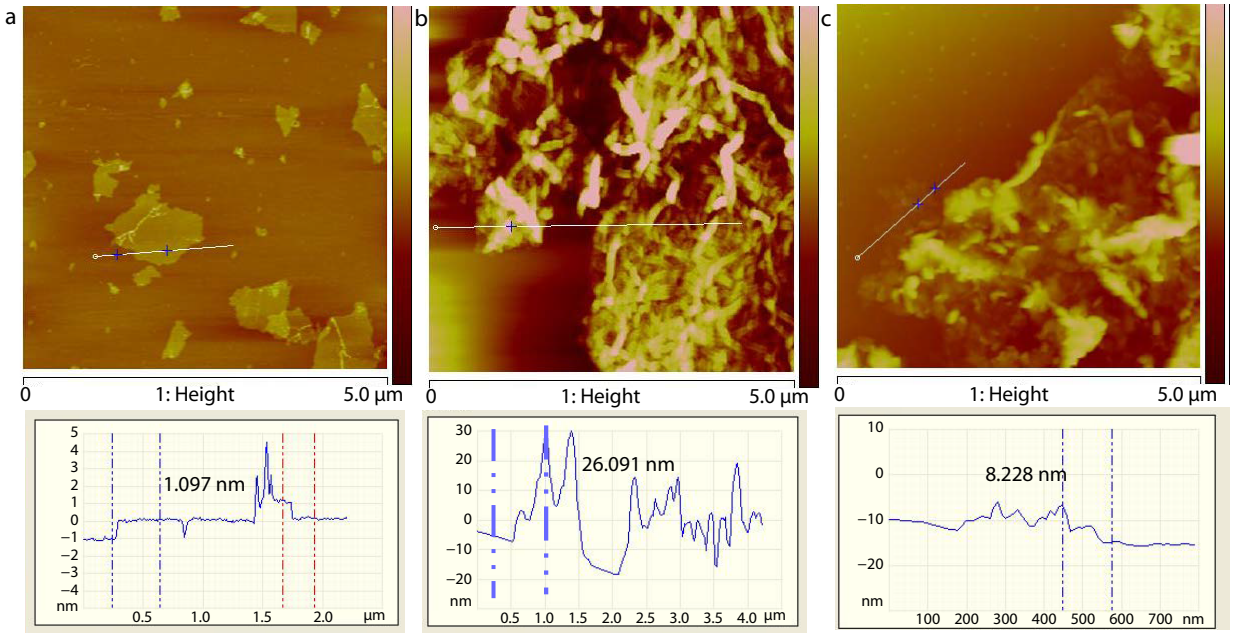

Fig. 3 AFM images and height profiles of (a) GO, (b) GNS and (c) GNS-LDH.

in color, and the addition of 0.5 wt%–2 wt% GNS changes the color of the film completely to black. With the addition of 0.5 wt% GNS-LDH, the composite becomes a translucent film, and the color intensifies with increasing addition. However, its color was lighter than that of the GNS-based polymer at the same level. No obvious black spots were observed on any of the films, indicating that GNS-LDH was dispersed uniformly in the matrix macroscopically.

The dispersion of GNSs and GNS-LDH in ABS was observed using SEM and TEM. Figs. 5(a) and 5(b) show the frozen-section SEM images of the ABS/GNS2 and ABS/GNS-LDH2 composites, respectively. The fracture surface of pure ABS was relatively smooth (not shown). In contrast, the fracture surface of the ABS/GNS2 composites was rougher, and individual graphene flakes could be observed in some areas, probably because of the weak interfacial forces between the graphene and ABS matrix, which were removed from the matrix during brittle fracture. The surface of the ABS/GNS-LDH2 composite

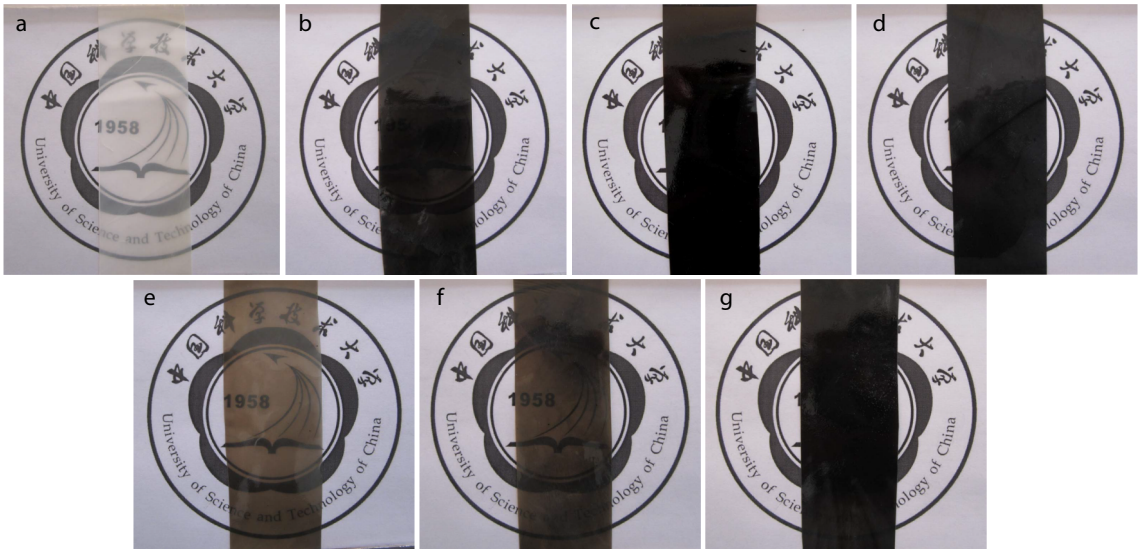

Fig. 4 Photographs of (a) ABS, (b) ABS/GNS0.5, (c) ABS/GNS1, (d) ABS/GNS2, (e) ABS/GNS-LDH0.5, (f) ABS/GNS-LDH1 and (g) ABS/GNS-LDH2 composite films.

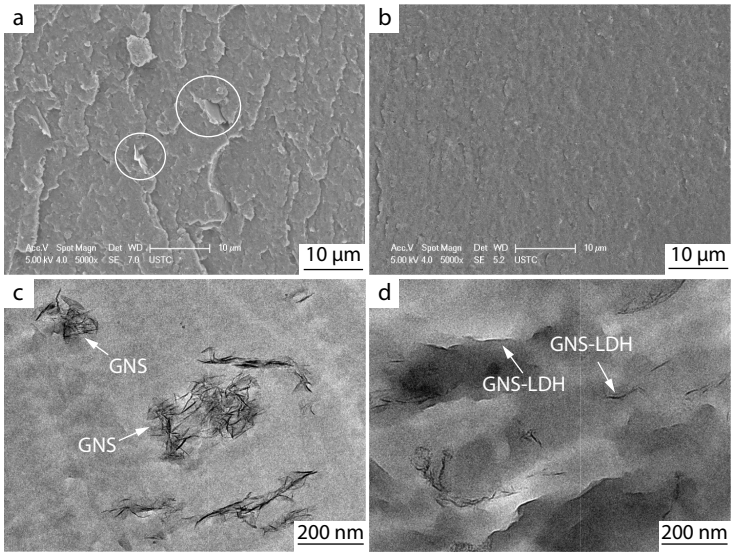

Fig. 5 SEM images of the fractured surfaces of the (a) ABS/GNS2 and (b) ABS/GNS-LDH2 composites; TEM images of the (c) ABS/GNS2 and (d) ABS/GNS-LDH2 composites.

system was smoother with no obvious agglomeration, and the heteroconjugates were well dispersed and embedded in the matrix. Figs. 5(c) and 5(d) show the TEM images of ultrathin sections of the ABS/GNS2 and ABS/GNS-LDH2 composites, respectively. The black stripes in the figures represent the side views of the graphene flakes. In general, graphene is well dispersed in the matrix; however, some stacking still occurs locally. In addition, GNS-LDH exhibits an intercalation-exfoliation state in the matrix, which achieves molecular-level dispersion. These results indicate that the introduction of NiFe-LDH can hinder the agglomeration of GNSs and promote their dispersion in the ABS matrix to form nanocomposites.

Mechanical Properties of the ABS/GNS-LDH Nanocomposites

Table 1 lists the compositions of the ABS composites and their corresponding mechanical properties. Compared with that of the ABS resin, the tensile strength of all the composites improved, but the elongation at break gradually decreased with increasing addition amount. The tensile strength of the ABS/GNS composites slightly increased to 36.05, 37.38, and 37.12 MPa with the addition of 0.5 wt%, 1 wt%, and 2 wt% graphene, respectively, and the tensile strength of the composites reached 41.1 MPa with the addition of 0.5 wt% GNS-LDH, which was greater than the increase of 0.5 wt% GNS-LDH in the ABS/GNS-LDH system. The tensile strength of the composites reached 41.1 MPa after adding only 0.5 wt% GNS-LDH, which increased by 25%. With the addition of 1 wt% GNS-LDH, the tensile strength of the material reached a maximum value of 46.23 MPa, which is an increase of 39%. The tensile strength of the material decreased slightly when the hybrid content was increased further. This indicates that there is a critical value for

graphene-based materials added to the matrix at which the mechanical properties are optimal, which is in line with previous reports on polymers reinforced with carbon nanomaterials.[21,22] However, with the addition of GNS-LDH, there is an inevitable deterioration in the elongation at break of the material, which is often observed in carbon-material-reinforced matrices.[23]

The effect of nanofillers on the flexural strength of the ABS systems was examined in a similar manner. As shown in Table 1, the flexural properties of the composites, whether GNS or GNS-LDH, were greater than those of the pure matrix (39 MPa), and increased with increasing pressure. The reinforcement effect of GNS-LDH on ABS was greater than that of GNS at the same additive amount, and the tensile strength of ABS increases to 56.79 MPa, which was 45.6% when the additive amount of GNS-LDH was 2.0 wt%. The obvious improvement in the mechanical properties of the materials also proves that GNS-LDH is well dispersed in the ABS matrix, which is attributed to the fact that the introduction of NiFe-LDH inhibits the re-agglomeration of GNS and promotes exfoliation in the matrix.

Fig. 6 shows the energy-storage modulus curves of the ABS composites. The energy storage modulus of ABS was approximately 1.8 GPa at 40 °C. The energy storage modulus and tensile strength of the composites tended to increase but then decreased with increasing nanofiller content. Compared with the same GNS-LDH content, the increase in the energy storage modulus was more obvious. At 1 wt% GNS-LDH, the energy storage modulus of the material reaches 2.38 GPa, which is an increase of 31.7%. In addition, T_g of the material increased with the addition of either GNS or GNS-LDH, which was attributed to the limited mobility of the ABS chains by the graphene hybrids.[24]

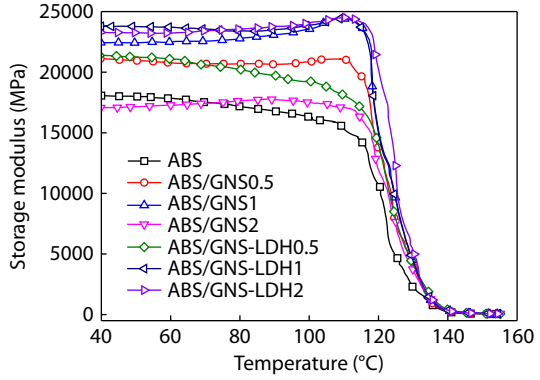

Fig. 6 Storage modulus (E') plots of ABS and its nanocomposites with various GNS and GNS-LDH contents.

Thermal Stability of the ABS/GNS-LDH Nanocomposites

Fig. 7 shows the TGA curves of ABS and its composites under nitrogen; the relevant data are listed in Table 2. ABS undergoes one-step thermal degradation under nitrogen, which mainly occurs at 300–550 °C, and corresponds to the process of random breakage of molecular chains, which is essentially residue-free at high temperatures. The addition of a small amount of GNS slightly increased the $T_{-5\%}$ of the material, which may be related to the sheet-barrier effect of graphene. The char formation of the ABS/GNS composites at high temperatures gradually increased with the addition of GNS, and the addition of GNS-LDH decreased $T_{-5\%}$ of the material, which may be related to the early decomposition and dehydration of NiFe-LDH when subjected to heat. However, the residual amount of the material increased significantly with an increase in NiFe-LDH. According to the local amplification curve, the residual amount of ABS/GNS-LDH composites gradually increased from 4.5 wt% to 12.2 wt%, which indicates that GNS-LDH can effectively promote the char formation of ABS. From the DTG curve, the maximum thermal decomposition rate of ABS/GNS-LDH decreased, and the decrease became increasingly obvious with increasing addition amounts, which indicated that GNS-LDH could delay the degradation of ABS. The improvement in the thermal stability of the ABS/GNS-LDH composites was attributed to the following two factors: the homogeneous dispersion of GNS formed a good physical barrier layer, which could prevent the escape of volatile gases and diffusion of oxygen.[25] The improved thermal stability of the ABS/GNS-LDH composites can be attributed to two factors: the uniform dispersion of GNS forms a good physical barrier layer, which can prevent the escape of volatile gases and the diffusion of oxygen, and the loaded NiFe-LDH can catalyze the formation of char from cracking products.[5,26]

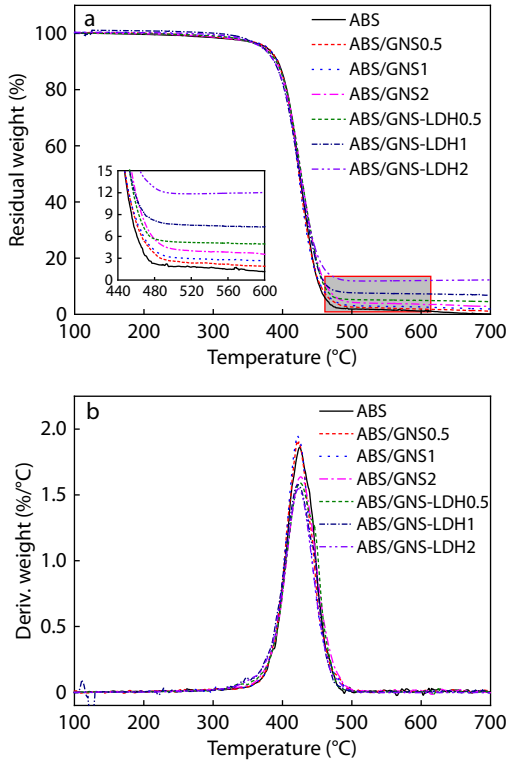

Fig. 7 (a) TG and (b) DTG curves of ABS and its nanocomposites at various loadings in nitrogen.

Flame Retardant Properties of ABS/GNS-LDH Nanocomposites

Fig. 8 shows the temperature dependence curves of the heat release rates of the ABS and its nanocomposites, and the specific parameters are listed in Table 3. A sharp peak appeared when the pure ABS was burned, and the peak heat release rate (PHRR) was 556 W/g. The PHRR of the material decreased gradually with the increasing addition of GNS, which was related to the

Table 2 TGA data of ABS and its nanocomposites with GNS and GNS-LDH in nitrogen.

Sample	$T_{-5\%}$ (°C)	$T_{-50\%}$ (°C)	T_{max} (°C)	Char residue (700 °C)
ABS	376.4	425.0	425.0	0.1
ABS/GNS0.5	377.2	423.6	423.9	1.1
ABS/GNS1	378.1	423.0	421.9	1.9
ABS/GNS2	373.0	427.0	426.3	2.9
ABS/GNS-LDH0.5	371.7	427.0	425.5	4.5
ABS/GNS-LDH1	371.8	424.4	422.4	6.8
ABS/GNS-LDH2	370.1	425.6	423.4	12.2

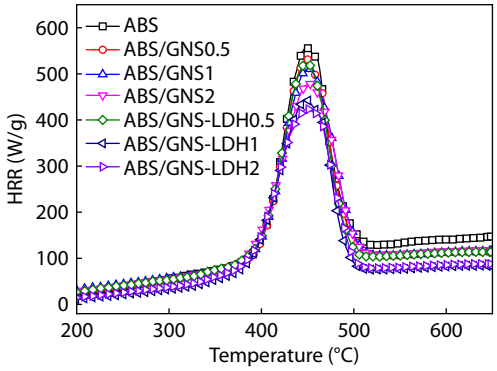

Fig. 8 Heat release rate versus temperature curves for ABS and its nanocomposites.

barrier of cracking gases by the GNS.[27] Compared with that of the ABS/GNS composites, the PHRR of the ABS/GNS-LDH composites with the same GNS-LDH content was lower and decreased with increasing GNS-LDH content. For example, at 2 wt% GNS-LDH, the PHRR of the composites decreased to 371.5 W/g, which was 33.2% lower than that of pure ABS. Table 3 shows that the PHRR of the ABS/GNS composite decreased to 371.5 W/g. Heat release capacity (HRC) is defined as the peak heat release rate per unit temperature rise. The lower the value, the better the flame retardancy.

As shown in Table 3, the total heat release (THR) of the ABS/GNS composites did not change significantly compared to that of the pure samples, indicating that most of the resin was consumed during combustion. The THR of the ABS/GNS-LDH system, however, decreased to a certain extent, with a THR value of 29.9 kJ/g at 2 wt% addition, which is a decrease of 12.3%. GNS-LDH acts as a flame retardant by promoting the formation of char during the combustion of ABS and reducing the escape of volatile gases.[28]

Table 3 MCC data of ABS and its nanocomposites with GNS and GNS-LDH.

Sample	HRC (J/(g·K))	PHRR (W/g)	THR (kJ/g)	Temp. (°C)
ABS	557	556	34.1	447.6
ABS/GNS0.5	459	460.8	33.2	448.5
ABS/GNS1	442	438.9	34.1	450.0
ABS/GNS2	405	406.3	33.1	450.3
ABS/GNS-LDH0.5	452	451.5	32.8	446.4
ABS/GNS-LDH1	395	395.7	29.3	447.9
ABS/GNS-LDH2	370	371.5	29.9	449.5

Flame Retardant Mechanism

The TG/FTIR coupling technique can be used to investigate the changes in the volatile gas products generated during the pyrolysis of the samples. Fig. 9 shows three-dimensional diagrams of the TG/FTIR results for the ABS and ABS/GNS-LDH pyrolysis processes. The infrared absorption spectra of all volatile products produced by cracking as a function of time are shown. The sample started to produce cracking gases at 22.1 min, and the characteristic absorption peaks appeared mainly in the following wavenumber ranges: 3300–2800, 2250–2400, 1800–1450 and 900–700 cm^{-1}.

Fig. 10(a) shows the infrared spectra of the gas-phase products of ABS and ABS/GNS-LDH2 at the maximum degradation rate. The possible cleavage products can be identified by several characteristic absorption peaks: hydrocarbons (3069 and 2930 cm^{-1}), CO_2 (2362 cm^{-1}), olefinic compounds (1599 cm^{-1}), and aromatic compounds (772 cm^{-1}).[29] The gas-phase compositions of the two samples are similar, but the overall gas-phase product concentration of ABS/GNS-LDH is much lower than that of ABS. Figs. 10(b)–10(d) show the characteristic gas-phase products of the two cracks as functions of time. Al-

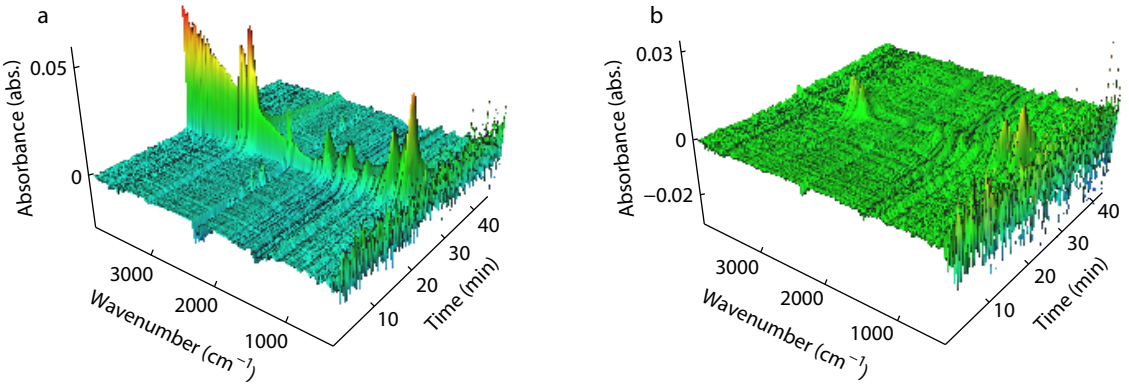

Fig. 9 3D diagrams of the gaseous volatiles in the thermal pyrolysis of (a) neat ABS and (b) ABS/GNS-LDH2.

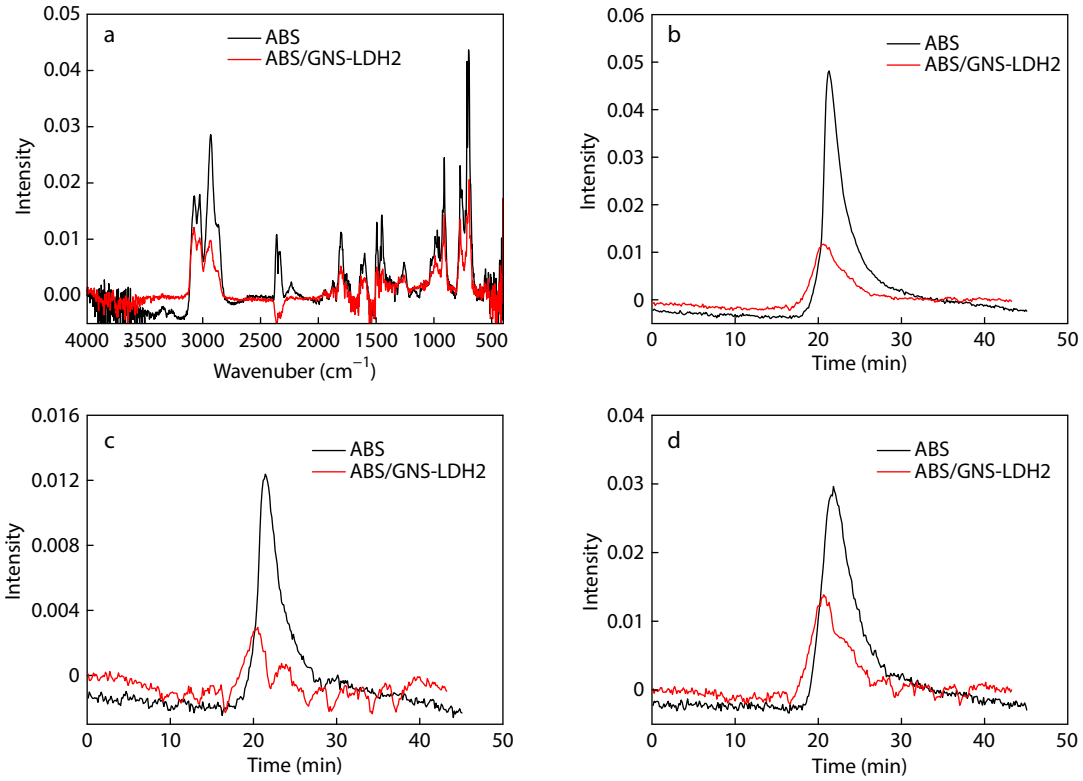

Fig. 10 (a) FTIR spectra of gaseous products at the maximum evolution rate and (b) hydrocarbons, (c) alkenes, and (d) aromatic compounds versus time from ABS and ABS/GNS-LDH2 nanocomposites.

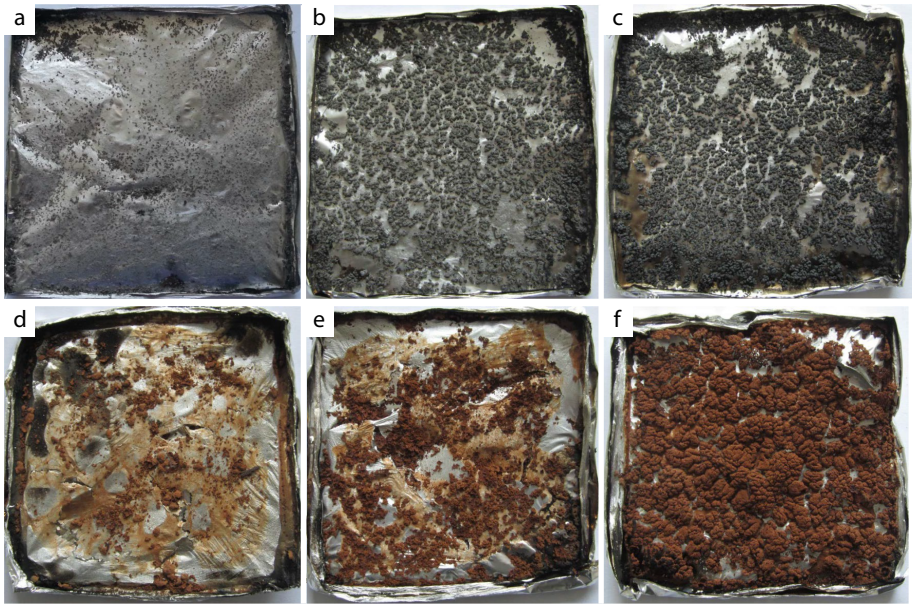

Fig. 11 Digital photographs of the char residues of the (a) ABS/GNS0.5, (b) ABS/GNS1, (c) ABS/GNS2, (d) ABS/GNS-LDH0.5, (e) ABS/GNS-LDH1, and (f) ABS/GNS-LDH2 nanocomposites.

though the cracking time of the ABS/GNS-LDH2 composite was slightly shorter, the concentration of several typical cracking products was much lower than that of ABS. Owing to the presence of GNS-LDH, the concentration of flammable volatile gases, such as hydrocarbons, olefins, and aromatic compounds, is reduced, thereby reducing the rate of heat release from the material.

Several studies have reported the use of carbon materials as flame-retardant additives in polymers. For example, CNTs form a network-like nanostructure during matrix combustion, blocking the escape of volatile gases and the diffusion of oxygen, thus providing a good flame-retardant effect.[30]

Graphene, with its large specific surface area and lamellar barrier, also exerts a flame-retardant effect, mainly in the con-

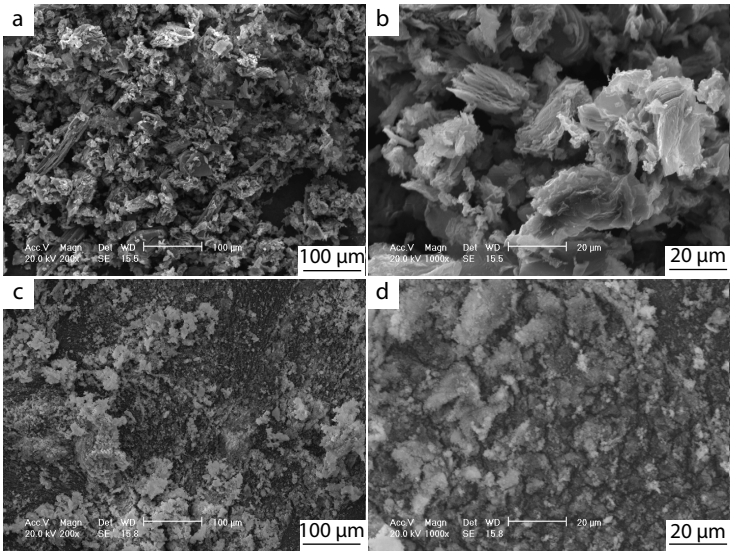

Fig. 12 SEM images of the char residues of the (a, b) ABS/GNS2 and (c, d) ABS/GNS-LDH2 nanocomposites.

densed phase. The flame retardancy of a material is closely related to the quality of the char layer; the higher the char residue content, the denser and stronger the char layer, and the slower the combustion process, the better the flame retardancy of the material.[31] Photographs of the charcoal residue after the cone calorimetric test were taken, and are shown in Fig. 11. Pure ABS burned vigorously without any residue (data not shown). When a small amount of GNS was added, the sample contained only a small amount of uniformly distributed residue in the form of loose silos. As the amount of added GNS increased, the residue became denser, but cracks and pores remained. In contrast, the ABS/GNS-LDH composite formed a brown char residue after combustion, which became denser and stronger with increasing GNS-LDH content, and was greater than that of ABS/GNS at the same content. GNS-LDH promotes the charring of the ABS matrix during combustion to form a protective char layer, which prevents the volatilization of gases and diffusion of oxygen.

The microscopic morphology of the char layer was further investigated using SEM, as shown in Fig. 12. SEM of the ABS/GNS2 char slag revealed that a network structure formed after combustion, but there were obvious gaps and holes (Fig. 12a). The enlarged SEM images show that the char slag consists of many layered structures that are derivatives of graphene. However, the surface of the graphene was relatively smooth, with almost no change in morphology and no additional carbon generation (Fig. 12b). In contrast, ABS/GNS-LDH2 formed a continuous and dense char layer after burning, and most of the GNS-LDH was encapsulated in the char layer (Fig. 12c). Under high-magnification SEM, the tightly packed charcoal particles on the surface of GNS-LDH formed an effective barrier (Fig. 12d). In this sense, GNS-LDH has a flame-retardant effect by promoting the formation of a dense and strong charcoal layer on the substrate, which blocks the volatilization of flammable gases and the diffusion of oxygen into the bottom material.

CONCLUSIONS

GNS-LDH hybrids and ABS/GNS-LDH composites with various additions were successfully prepared through *in situ* hydrothermal reactions and solution blending methods, with graphene as a reference. GNS-LDH significantly influences the mechanical properties, thermal stability, and flame retardancy of ABS composites, and the flame-retardant mechanism has been revealed from both gas and condensed phase perspectives. Among them, the unique structure of GNS-LDH, with its hard skeleton and catalytic detoxification properties, enables structural integration with the soft ABS matrix, endowing the composites with excellent comprehensive performance. The ABS/GNS-LDH composites exhibited a uniform dispersion. SEM and TEM images revealed molecular-level exfoliation of NiFe-LDH in the matrix. Mechanical tests revealed that compared with GNSs, GNS-LDH improved the tensile and flexural strengths more effectively. At 1 wt% GNS-LDH, the tensile strength increased by 39% and the flexural strength increased by 36.3%. DMA tests indicated an increased storage modulus. The TGA results demonstrated an improved thermal stability. Compared with ABS, the residue of the ABS/GNS-LDH2 composite increased to 12.2 wt%. The MCC and CONE results indicate better flame retardancy for the ABS/GNS-LDH composites than for the ABS/GNS composites with the same content. The TG/FTIR results revealed that the GNS-LDH promoted char formation, reduced volatile gas escape, and achieved flame retardancy. The ABS/GNS-LDH composites, with their enhanced mechanical properties, improved thermal stability, and remarkable flame retardancy, hold great potential for application in fields requiring high-performance materials.

Conflict of Interests

The authors declare no interest conflict.

Electronic Supplementary Information

Electronic supplementary information (ESI) is available free of charge in the online version of this article at http://doi.org/10.1007/s10118-026-3762-y.

Data Availability Statement

The data supporting the findings of this study are available from the author upon request. E-mail: wxcmx@ustc.edu.cn.

ACKNOWLEDGMENTS

This work was financially supported by Research on key technologies for the nationalization of offshore wind power cable for ultra-high voltage of 500kV and above (No. Y26-02), and Key Technology Research and Product Development of Power Cable System with Rated Voltage of 750 kV (No. Y23-03).

REFERENCES

1 Zhou, F.; Tang, W.; Xi, W.; Qian, L.; Wang, J.; Qiu, Y.; Chen, Y. Improving the fracture toughness, flame retardancy and smoke suppression of ABS by core-shell elastic flame retardant particles with P/Si synergistic effect. *Polym. Degrad. Stabil.* **2024**, *228*, 110893.
2 Amarnath, N.; Appavoo, D.; Lochab, B. Eco-friendly halogen-free flame retardant cardanol polyphosphazene polybenzoxazine networks. *ACS Sustain. Chem. Eng.* **2018**, *6*, 389–402.
3 Hu, X.; Luo, Y.; Liu, W.; Sun, Z. Synergistic interaction between inorganic layered materials and intumescent fire retardants for advanced fire protection. *Carbon* **2022**, *187*, 290–301.
4 Shi, X. H.; Shi, H.; Li, X. L.; Wu, S. J.; Xie, W. M.; Wang, D. Y. Polydopamine-primed FeCo-LDH endowed epoxy resin with enhanced flame retardancy and mechanical properties. *Constr. Build. Mater.* **2024**, *439*, 137070.
5 Wang, Q.; O'Hare, D. Recent advances in the synthesis and application of layered double hydroxide (LDH) nanosheets. *Chem. Rev.* **2012**, *112*4124-4155
6 Matusinovic, Z.; Wilkie, C. A. Fire retardancy and morphology of

Graphical Abstract

Effect of Graphene/Nickel-iron Layered Double Hydroxide Hybrids on the Thermal Decomposition and Flame Retardancy of Acrylonitrile-butadiene-styrene Copolymer Composites

Ning-Ning Hong , Jing-Ping Liu, and Xin Wang

Shanghai Electric Cable Research Institute Co., Ltd.; University of Science and Technology of China

A novel synergistic structure (GNS-LDH) was synthesized by modifying graphene with layered double hydroxide hybrids *via* hydrothermal method. The introduction of GNS-LDH imparted ABS with enhancement and toughening, flame retardancy and smoke suppression, and a reduction in toxicity, which promoted char formation, reducing volatile gas escape and achieving flame retardancy.

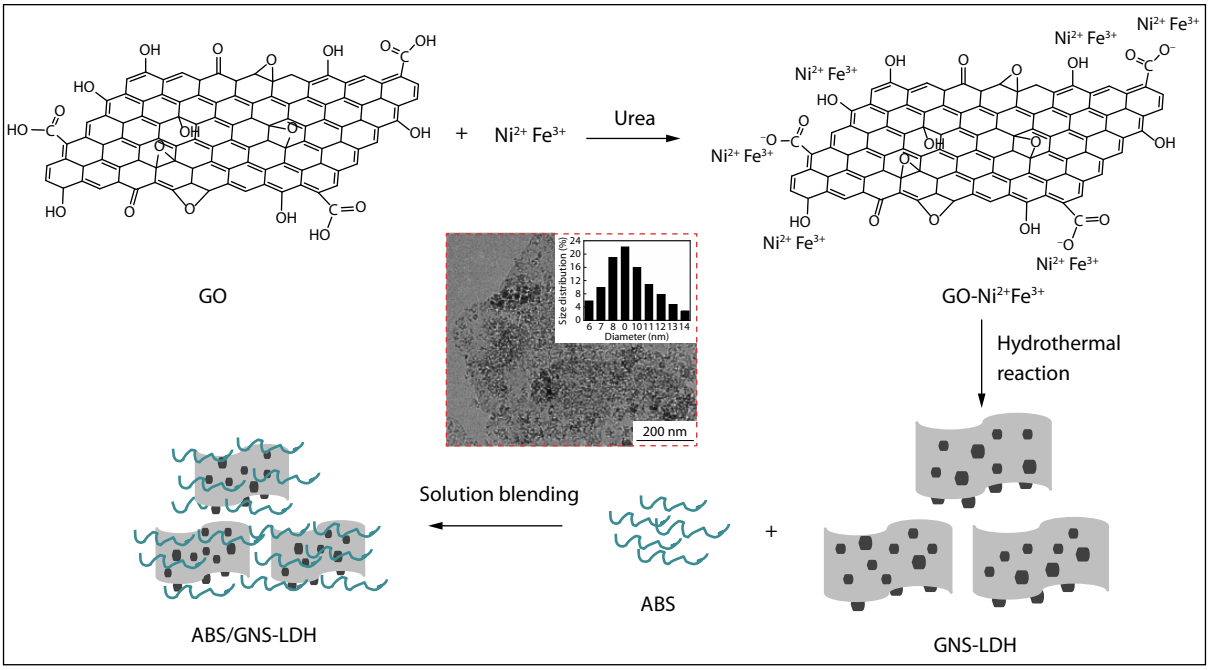

Chinese J. Polym. Sci., 2026 *https://doi.org/10.1007/s10118-026-3762-y*

layered double hydroxide nanocomposites: a review. *J. Mater. Chem.* **2012**, *22*, 18701.
7 Manzi-Nshuti, C.; Wang, D.; Hossenlopp, J. M.; Wilkie, C. A. The role of the trivalent metal in an LDH: synthesis, characterization and fire properties of thermally stable PMMA/LDH systems. *Polym. Degrad. Stabil.* **2009**, *94*, 705−711.
8 Manzi-Nshuti, C.; Wang, D.; Hossenlopp, J. M.; Wilkie, C. A. Aluminum-containing layered double hydroxides: the thermal, mechanical, and fire properties of (nano)composites of poly-(methyl methacrylate). *J. Mater. Chem.* **2008**, *18*, 3091.
9 An, W.; Ma, J.; Xu, Q.; Zhang, H.; Wei, L.; Kim, K.-H.; Xu, Y. 3-D flower-like templated LDH-rGO as coating additive for flame retardant products. *J. Colloid Interface Sci*. **2023**, *631*, 89−100.
10 Song, K.; Bi, X.; Wang, D.; Pan, Y.-T.; Xie, M.; He, J.; Wang, D.-Y.; Yang, R. Porous liquids assisted *in-situ* generated Co-LDH@MOF heterostructure with abundant defects for flame retardant and mechanical enhancement in polyurea composites. *Chem. Eng. J.* **2024**, *495*, 153850.
11 Park, J. M.; Kwon, D. J.; Wang, Z. J.; Gu, G.-Y.; DeVries, K. L. Interfacial, fire retardancy, and thermal stability evaluation of graphite oxide (GO)-phenolic composites with different GO particle sizes. *Compos. Part B Eng.* **2013**, *53*, 290−296.
12 Gao, Z.; Wang, J.; Li, Z.; Yang, W.; Wang, B.; Hou, M.; He, Y.; Liu, Q.; Mann, T.; Yang, P.; Zhang, M.; Liu, L. Graphene nanosheet/Ni^{2+}/Al^{3+} layered double-hydroxide composite as a novel electrode for a supercapacitor. *Chem. Mater.* **2011**, *23*, 3509−3516.
13 Zhang, L.; Zhang, X.; Shen, L.; Gao, B.; Hao, L.; Lu, X.; Zhang, F.; Ding, B.; Yuan, C. Enhanced high-current capacitive behavior of graphene/CoAl-layered double hydroxide composites as electrode material for supercapacitors. *J. Power Sources* **2012**, *199*, 395−401.
14 Murtaza, H.; Zhao, J.; Tabish, M.; Wang, J.; Mubeen, M.; Zhang, J.; Zhang, S.; Fan, B. Protective and flame-retardant bifunctional epoxy-based nanocomposite coating by intercomponent synergy between modified CaAl-LDH and rGO. *ACS Appl. Mater. Interfaces* **2024**, *16*, 13114−13131.
15 Wang, R.; Zhang, S.; Hu, X.; Leng, Y.; Li, X.; Tao, B.; Xu, M. Constructing piperazine pyrophosphate@LDH@rGO with hierarchical core-shell structure for improving thermal conductivity, flame retardancy and smoke suppression of epoxy resin thermosets. *Compos. Part B Eng.* **2024**, *287*, 111870.
16 Li, H.; Zhu, G.; Liu, Z. H.; Yang, Z.; Wang, Z. Fabrication of a hybrid graphene/layered double hydroxide material. *Carbon* **2010**, *48*, 4391−4396.
17 Chua, C. K.; Pumera, M. Selective removal of hydroxyl groups from graphene oxide. *Chem* **2013**, *19*, 2005−2011.
18 Chen, Q.; Shi, S.; Liu, X.; Jin, L.; Wei, M. Studies on the oxidation reaction of l-cysteine in a confined matrix of layered double hydroxides. *Chem. Eng. J.* **2009**, *153*, 175−182.
19 Li, M.; Zhu, J. E.; Zhang, L.; Chen, X.; Zhang, H.; Zhang, F.; Xu, S.; Evans, D. G. Facile synthesis of NiAl-layered double hydroxide/graphene hybrid with enhanced electrochemical properties for detection of dopamine. *Nanoscale* **2011**, *3*, 4240−4246.
20 Zhao, X.; Zhang, Q.; Chen, D.; Lu, P. Enhanced mechanical properties of graphene-based poly(vinyl alcohol) composites. *Macromolecules* **2010**, *43*, 2357−2363.
21 Gonçalves, G.; Marques, P. A. A. P.; Barros-Timmons, A.; Bdkin, I.; Singh, M. K.; Emami, N.; Grácio, J. Graphene oxide modified with PMMA *via* ATRP as a reinforcement filler. *J. Mater. Chem.* **2010**, *20*, 9927−9934.
22 Park, S. H.; Bandaru, P. R. Improved mechanical properties of carbon nanotube/polymer composites through the use of carboxyl-epoxide functional group linkages. *Polymer* **2010**, *51*, 5071−5077.
23 Song, P.-A.; Xu, L.; Guo, Z.; Zhang, Y.; Fang, Z. Flame-retardant-wrapped carbon nanotubes for simultaneously improving the flame retardancy and mechanical properties of polypropylene. *J. Mater. Chem.* **2008**, *18*, 5083−5091.
24 Yadav, S. K.; Cho, J. W. Functionalized graphene nanoplatelets for enhanced mechanical and thermal properties of polyurethane nanocomposites. *Appl. Surf. Sci.* **2013**, *266*, 360−367.
25 Huang, G.; Gao, J.; Wang, X.; Liang, H.; Ge, C. How can graphene reduce the flammability of polymer nanocomposites. *Mater. Lett.* **2012**, *66*, 187−189.
26 Cao, Y.; Feng, J.; Wu, P. Polypropylene-grafted graphene oxide sheets as multifunctional compatibilizers for polyolefin-based polymer blends. *J. Mater. Chem.* **2012**, *22*, 14997−15005.
27 Chen, X.; Huo, L.; Jiao, C.; Li, S. TG–FTIR characterization of volatile compounds from flame retardant polyurethane foams materials. *J. Anal. Appl. Pyrolysis* **2013**, *100*, 186−191.
28 Kashiwagi, T.; Du, F.; Douglas, J. F.; Winey, K. I.; Harris, R. H. Jr, Shields, J. R. Nanoparticle networks reduce the flammability of polymer nanocomposites. *Nat. Mater.* **2005**, *4*, 928−933.
29 Bikiaris, D. Can nanoparticles really enhance thermal stability of polymers? Part II: an overview on thermal decomposition of polycondensation polymers. *Thermochim. Acta* **2011**, *523*, 25−45.
30 Liu, S.; Fang, Z.; Yan, H.; Chevali, V. S.; Wang, H. Synergistic flame retardancy effect of graphene nanosheets and traditional retardants on epoxy resin. *Compos. Part A Appl. Sci. Manuf.* **2016**, *89*, 26−32.
31 He, W.; Song, P.; Yu, B.; Fang, Z.; Wang, H. Flame retardant polymeric nanocomposites through the combination of nanomaterials and conventional flame retardants. *Prog. Mater. Sci.* **2020**, *114*, 100687.